ON OSCILLATING HYDROFOILS

Part II

by

S. Schuster and H. Schwanecke

June 1962

Contract N 62558-2552

Office of Naval Research

(6) ON OSCILLATING HYDROFOILS

Part II, (7) NA

(8) by

~~Prof. Dr. Ing.~~ S. Schuster, and ~~director, Berlin Towing Tank~~

~~Dr. Ing.~~ H. Schwanecke, ~~head, research department, Hamburg Model Basin~~
~~(formerly Berlin Towing Tank)~~

(9)

~~Berlin~~, June ~~1~~962, (10) 12 p. illus. tables, 1 refs.

(11) NA

Work sponsored by the Office of Naval Research

(12) Contract ~~N~~ N 62558 - 2552

(13) NA

1. Introduction

As already mentioned in the first part of the studies on oscillating hydrofoils (see: Part I, December 1960) the hydrodynamic forces acting on a hydrofoil running in a seaway can be split up into a steady component and into two nonsteady components.

The results of the theoretical and experimental investigations of the steady state of flow were reported in Part I; also those of experimental studies with two hydrofoil models, which could move in the vertical direction without any restrictions, running in head seas. This unsteady state of flow, which represents a hydrodynamically forced oscillation of the foils in the vertical direction, was formerly called "Unsteady case No. 3".

The present report contains the results of the experimental investigations of the above mentioned unsteady components of the hydrodynamic forces, i.e. the hydrodynamic exciting forces (Case No. 2) and the hydrodynamic masses and damping forces (Case No. 1). The tests were carried out with the same foil models, as described in Part I, namely a plane foil with an aspect ratio A = 5 and a chord length c = 0.1 m and a dihedral foil with the dihedral angle Ψ = 30 deg. and a chord length c = 0.1 m.

2. Measuring arrangements and measuring procedure

2. 1. Hydrodynamic exciting forces

The measurements of the hydrodynamic exciting forces generated by the orbital motions were taken in the deep water tank of VWS (cross section : 8.00 x 4.15 m^2). The hydrofoil models were fixed to the big six-component balance of VWS, working with inductive beam pickups. The six-component balance was installed on the carriage of the deep water tank. The sketch fig. 1 and the photograph fig. 3 show the dihedral foil model fixed to the balance. An ohmic device arranged sidewards of the foil models at a distance of about two meters was used as a wave recorder. Its sensing element was in line with the leading edge of the respective foil model. The signals of the

force pickups and of the wave recorder were registered by a recording oscillograph.

In the present research program hydrofoils in vertical oscillations should be tested. Therefore it was sufficient to measure only the lift. The electrical supply system of the inductive pickups did not allow the use of electrical filters to eliminate the "white noise" of the towing carriage and the measuring arrangement. Therefore the records were mechanically analysed afterwards. Only the first component of the unsteady lift was considered.

The flat foil was tested in four and the dihedral foil in three mean depths of submergence. The tests were made at a speed of about 6 m/s and in head seas. The geometrical angle of incidence for the chord of the profile amounted to $\alpha_{geom} = 1.8$ (1.6 ; 2.3) deg. for the flat foil and to $\alpha_{geom} = \alpha^*_{geom} \cos\vartheta = 1.9$ deg. for the dihedral foil, where α^*_{geom} is the geometrical angle of incidence measured in the vertical plane. The wave lengths were varied between $\lambda = 1.5$ m and $\lambda = 6.8$ m and the corresponding wave heights between $2a = 0.046$ m and $2a = 0.136$ m (a = wave amplitude). The test data are registered in tables No. 1 - 7.

2. 2 Hydrodynamic masses and hydrodynamic damping forces

These measurements were taken in the free-surface water tunnel of VWS. The water depth in the measuring section (adjustable bottom) had been adjusted to 0.7 m. Thus a cross section of the flow of about 1.3 m^2 resulted. The measuring apparatus is shown in figs. 2 and 4. The motion of the vertical supporting tube was exactly sinusoidal. Only the lift was measured. The force pickup consisted of a steel bar fitted with strain-gauges. For the measurement of the phase angle between the vertical oscillations and the resulting unsteady lift an inductive accelerometer was fixed to the foil models. The signals of the strain-gauges and of the accelerometer were registered by a recording oscillograph. To eliminate the "white noise" of the tunnel and of the measuring arrangement electrical filters were used.

The measurements were taken at four depth of submergence for either foil and at a speed in the test section of about 5 m/s. The geometrical angles of incidence amounted to $\alpha_{geom} = 1.8$ deg. for the flat foil and to $\alpha_{geom} = 1.9$ deg. for the dihedral foil. The frequencies of the vertical oscillations were chosen in such a way that the same range of the reduced frequencies μ was covered as for the measurements of the forces. The test data are registered in the tables No. 8-15.

2. 3. Forced vertical oscillations

The measurements of the hydrodynamically forced vertical oscillations of the hydrofoil models due to the orbital-motions have already been desribed in the first report (Part I) of the present research program. In addition, the test data are listed in the tables No. 16 and 17 of the present report.

3. Results

3. 1. Hydrodynamic exciting forces

The results of the tests are plotted in nondimensional form against the reduced frequency $\mu = \frac{\nu\, c}{2\, u_o}$ (ν = frequency of encounter), in fig. 5 - 7 for the flat foil and in fig. 8 - 10 for the dihedral foil.

Fig. 5 shows the coefficient of the mean lift for the flat foil

$$K_{Zo} = \frac{P_{Zo}\,(\mu)}{P_{Zo}\,(\mu = o)}. \qquad (1)$$

Within the range of the nondimensional depth of submergence $\bar{h} = \frac{h}{c} = 1.2 - 2.7$ the influence of the free surface is but small. The average of the measured values is somewhat below unity. That means a loss of mean lift occurs at the foil, when running in head seas. This loss of mean lift is caused by higher order effects in consequence of the nonsteady state of flow in addition to the steady state component, and of the horizontal component of the orbital motions. The influence of the magnitude of the wave amplitude on the mean lift, which is also a higher order effect, is not eliminated.

Fig. 6 shows the coefficient of the first order unsteady lift

$$K_{Z1} = \frac{|P_{Z1}(\mu)|}{\varrho u_o^2 bc 2\pi \alpha_W(\bar{h})} \qquad (2)$$

(nomenclature see section 6).

In this expression is

$$\alpha_W(\bar{h}) = \frac{|z_W(\bar{h})|}{u_o} = \frac{g}{u_W u_o} a \exp\left(-\frac{gc}{u_W^2}\bar{h}\right) \qquad (3)$$

the hydrodynamic angle of incidence resulting from the speed of advance and the amplitude of the orbital velocity.

For $1.2 \leq \bar{h} \leq 2.8$ the influence of the free surface on the lift amplitudes at low reduced frequencies is relatively small. With increasing reduced frequencies the free-surface effect increases too. As a comparison the theoretical curve valid for a hydrofoil of infinite aspect ratio infinitely deep submerged in a periodic unsteady velocity field containing only vertical additional flow components ([6]) is plotted in fig. 6. The curve is corrected by the steady state theory of W e i n i g ([4], see Part I) for the aspect ratio A = 5. Just as the tests described in [6] the measured values for the great depth and for increased reduced frequencies are higher even than the theoretical values for large aspect ratio. This could be the influence of the periodically alternating tip vortices, which produce higher local loads towards the foil tips. The influence of the geometrical angle of incidence seems to be small.

In fig. 7 the phase differences between the wave peaks when beeing above the centre of the chord and the respective maxima of the unsteady lift are shown.

Fig. 8 shows the coefficient of the mean lift (according to equ. (1)) for the dihedral foil. Partly the measured values are considerably below unity. That means a loss of mean lift which increases with decreasing depth of immersion $\bar{h}_2$ resp. with decreasing effective aspect ratio.

The coefficient of the first order unsteady lift for the dihedral foil is shown in fig. 9. It is defined by

$$K_{Z1} = \frac{|P_{Z1}(\mu)|}{\varrho u_o^2 bc 2\pi \cos\vartheta \alpha_W (0.7\,\bar{h}_2)} \tag{4}$$

with

$$\alpha_W(0.7\,\bar{h}_2) = \frac{g}{u_W u_o} a \exp\left(-0.7\,\frac{gc}{u_W^2}\,\bar{h}_2\right). \tag{5}$$

Fig. 10 shows the phase differences between the wave peaks when beeing above the centre of the chord and the respective maxima of the unsteady lift. Owing to the influences of the free surface and of the reduction in effective aspect ratio with decreasing depth of immersion, the phase angle varies considerably with the depth $\bar{h}_2$.

3. 2. Hydrodynamic masses and hydrodynamic damping forces

The results of these tests are plotted in nondimensional form against the reduced frequency in fig. 11 and 12 for the flat foil and in fig. 13 and 14 for the dihedral foil.

Fig. 12 shows the nondimensional unsteady lift-amplitudes for the flat foil

$$G_Z = \frac{|P_Z(\mu)|}{\varrho u_o^2 b 2\pi\ z_o} \tag{6}$$

with z_o = amplitude of vertical oscillation.

The influence of the free surface nearly corresponds with that of the steady state of flow reported in Part I. For greater depths of submergence the measured lift-amplitudes are partly higher than those calculated by means of the steady state correction for the finite aspect ratio. Therefore within certain ranges of the reduced frequency the unsteady diminution of the lift amplitudes due to the finite aspect ratio seems to be smaller than the steady state diminution.

The phase difference between the vertical oscillation and the respective maximum of the unsteady lift is shown in fig. 12 For the depths of submergence $\bar{h} = 1.0 - 1.9$ the phase differences measured are smaller than those calculated for

infinite aspect ratio. At the depth $\bar{h} = 0.5$ and at small reduced frequencies the measured phase difference is bigger than the calculated phase difference. That means a magnification of the phase angle with decreasing depth of submergence for small reduced frequencies.

Fig. 13 shows the nondimensional lift amplitudes for the dihedral foil

$$G_Z = \frac{|P_Z(\mu)|}{\varrho u_o^2 b 2\pi \cos \vartheta_{z_o}} . \qquad (7)$$

Owing to the decreasing effective aspect ratio with decreasing depth of immersion, the influence of the immersion on the lift is big.

The phase angle between the vertical oscillation and the respective maximum of the unsteady lift experiences a large reduction at small depths of immersion. This can be seen in fig. 14. Since there is an increase of the phase angle due to the surface influence, the reduction is a consequence of the low effective aspect ratio.

The hydrodynamic masses and hydrodynamic damping forces acting on the oscillating foils can be derived from the results presented in fig. 11 - 14. In the nondimensional form

$$G_Z \exp (i \vartheta_Z)$$

the real part, divided by ν^2, is proportional to the hydrodynamic mass and the negative imaginary part, divided by ν, proportional to the hydrodynamic damping force. Thus

$$m_h = \frac{|P_Z(\mu)| \cos \vartheta_Z}{z_o \nu^2} \qquad \text{(hydrodynamic mass)}$$

$$d_h = - \frac{|P_Z(\mu)| \sin \vartheta_Z}{z_o \nu} \qquad \text{(hydrodynamic damping force).} \qquad (8)$$

The hydrodynamic masses and the hydrodynamic damping forces are plotted against the reduced frequency in fig. 15 and 16 for the flat foil in the following form

$$\frac{m_h}{\rho u_o^2 b 2\pi} = \frac{G_Z \cos\vartheta_Z}{\nu^2}$$

$$\frac{d_h}{\rho u_o^2 b 2\pi} = -\frac{G_Z \sin\vartheta_Z}{\nu} \quad . \tag{9}$$

Fig. 17 and 18 show the respective expressions for the dihedral foil

$$\frac{m_h}{\rho u_o^2 b 2\pi \cos\vartheta} = \frac{G_Z \cos\vartheta_Z}{\nu^2}$$

$$\frac{d_h}{\rho u_o^2 b 2\pi \cos\vartheta} = -\frac{G_Z \sin\vartheta_Z}{\nu} . \tag{9a}$$

Because of the low reduced frequencies the magnitude of the hydrodynamic masses is small (fig. 15 and 17). The influence of the free surface is considerable. The opposite tendencies of the magnitudes of the hydrodynamic masses at low depths $\bar{h}$ and $\bar{h}_2$ show the big influence of the effective aspect ratio. With the exception of the small depth of immersion for the dihedral foil the hydrodynamic masses become negative with decreasing reduced frequencies. That means a virtual diminution of the masses of the foils within this range of reduced frequencies.

The hydrodynamic damping forces of the foils are shown in fig. 16 and 18. Near $\mu = 0.14$ the influence of the free usrface has a maximum which decreases with decreasing depths of submergence (fig. 16). The hydrodynamic damping force for the dihedral foil decreases with decreasing depth of immersion. There is no noteworthy dependence on the reduced frequency.

4. Hydrodynamically forced oscillation

With the results of section 3 and the results of the steady state measurements referred to in Part I, the equation of motion for a hydrofoil running near the free surface in a seaway, when linearity will b assumed and only first oder harmonics will be taken into account, can be written in the form

$$(m + m_h) \ddot{z}_F(t) + d_h \dot{z}_F(t) + \frac{dP_{Zo}(\bar{h})}{dh} z_F(t) = \left|P_{Z1}\right| \exp (i\nu t + i\vartheta_{Z1}). \qquad (10)$$

$$(P_{Zo} \equiv L).$$

With

$$z_F(t) = \left|z_F\right| \exp (i\nu t + i\psi) \qquad (11)$$

follows from (10)

$$\psi = \vartheta_{Z1} - \tan^{-1}\left(\frac{\nu d_h}{\frac{dP_{Zo}(\bar{h})}{dh} - \nu^2 (m + m_h)} \right) \qquad (12)$$

and

$$\left| z_F \right| = \frac{\left|P_{Z1}\right|}{\sqrt{\left(\frac{dP_{Zo}(\bar{h})}{dh} - \nu^2(m + m_h)\right)^2 + \nu^2 d_h^2}} \qquad (13)$$

Thus

$$z_F(t) = \frac{\left|P_{Z1}\right|}{\sqrt{\left(\frac{dP_{Zo}(\bar{h})}{dh} - \nu^2(m + m_h)\right)^2 + \nu^2 d_h^2}} \cdot \exp\left(i\vartheta_{Z1} - i \tan^{-1}\left(\frac{\nu d_h}{\frac{dP_{Zo}(\bar{h})}{dh} - \nu^2(m + m_h)} \right) + i\nu t \right) \qquad (14)$$

The steady state mean lift has the magnitude

$$P_{Zo}(\bar{h}) = \rho u_o^2 bc 2\pi\alpha K_\alpha K_A K_P K_{\bar{h}} K_{Zo}$$

with K_α, K_A, K_P, and $K_{\bar{h}}$ defined in Part I. (15)

and $\alpha K_\alpha = \alpha_{geom} + 2m$.

The "hydrodynamic spring constants" in equ. (12) - (14) are then expressed by

$$\frac{dP_{Zo}(\bar{h})}{dh} = \frac{1}{c} \frac{dP_{Zo}(\bar{h})}{d\bar{h}} \qquad (16)$$

$$= \rho u_o^2 b 2\pi\alpha K_\alpha K_A K_P \frac{d}{d\bar{h}} (K_{Zo} K_{\bar{h}}) \quad \text{for the flat foil}$$

and

$$\frac{dP_{Zo}(\bar{h}_2)}{dh} = \varrho u_o^2 2\pi\alpha K_\alpha \; K_P \frac{d}{d\bar{h}} \left(b K_A K_{Zo} K_{\bar{h}_m} \right) \qquad (16a)$$

respectively for the dihedral foil.

In equ. (16), (16a) are

$$\frac{d}{d\bar{h}} \left(K_{Zo} K_{\bar{h}} \right) = K_{Zo} \frac{dK_{\bar{h}}}{d\bar{h}} + K_{\bar{h}} \frac{dK_{Zo}}{d\bar{h}} \qquad (17)$$

and

$$\frac{d}{d\bar{h}} \left(b K_A K_{Zo} K_{\bar{h}_m} \right) = bK_{Zo} K_A \frac{dK_{\bar{h}_m}}{d\bar{h}} + bK_{Zo} K_{\bar{h}_m} \frac{dK_A}{d\bar{h}} + \qquad (17a)$$

$$+ bK_A K_{\bar{h}_m} \frac{dK_{Zo}}{d\bar{h}} + K_{Zo} K_A K_{\bar{h}_m} \frac{db}{d\bar{h}}$$

with

$$\frac{dK_A}{d\bar{h}} = \frac{dK_A}{dA} \frac{2}{tg\,\vartheta} \qquad (18)$$

$$\frac{db}{d\bar{h}} = \frac{c}{\sin\vartheta}$$

5. Examples

Now the forced oscillations of the two hydrofoil models running at a speed $u_o \triangleq 6.0$ m/s in head seas as described in section 2.3 (tables 16, 17) will be calculated by means of the linear theory and for a first harmonic excitation.

For the flat foil (P = 11.8 kp) the mean depth of submergence $\bar{h} = 0.50$ and for the dihedral foil (P = 15.0 kp) the mean depth of immersion $\bar{h}_2 = 1.37$, according to an effective mean aspect ratio A = 5.5, will be considered. The factors K_A, $K_{\bar{h}}$, $K_{\bar{h}_m}$, dK_A/dA, $dK_{\bar{h}}/d\bar{h}$ and $dK_{\bar{h}_m}/d\bar{h}$ will be taken from Part I (steady state) and the factors K_{zo}, $dK_{zo}/d\bar{h}$ from fig. 5 and 8, whereby for $\bar{h} = 0.50$ the values of K_{zo} and $dK_{zo}/d\bar{h}$ in fig. 5 must be extrapolated.

The expressions (17) and (17a) then result to

$$\frac{d}{d\bar{h}} \left(K_{Zo} K_{\bar{h}} \right) = 0.74$$

$$\frac{d}{d\bar{h}} \left(bK_A K_{Zo} K_{\bar{h}_m} \right) = 0.12$$

(for the first approximation the factor K_{zo} can be taken as independent from μ when μ is small).

With the profile efficiency assumed to be

$$K_p = 0.97$$

the "hydrodynamic spring constants" according to equ. (16) and (16a) in this special case result to

$$\frac{dP_{Zo}(\bar{h})}{d\bar{h}} = 178 \text{ kp/m} \qquad \text{(flat foil)}$$

and $$\frac{dP_{Zo}(\bar{h}_2)}{d\bar{h}} = 58 \text{ kp/m} \qquad \text{(dihedral foil).}$$

The heave amplitudes according to equ. (13) and the phase angles between the wave-peaks and the respective maxima of heave are shown in fig. 19 and 20. In the same figures the measured heave amplitudes and phase angles (see Part I) are presented for comparison.

There are big differences between the measured and calculated amplitudes of heave (fig. 14). The differences increase with decreasing reduced frequencies, i.e. with increasing wave lengths. Here additional effects, for example the nonlinearity of the "hydrodynamic spring constants", the effect of varying depth of water above the foils, the interaction of the exciting forces, i.e. the influence of the orbital motions on the hydrodynamic forces on the oscillating foil specially on the hydrodynamic damping forces, the influence of higher oder harmonics of the exciting forces etc.seem to be not neglegible.

The measured phase angles are about 30 degrees more negative than the calculated ones (fig. 20). This difference is only slightly dependent on the reduced frequency and has nearly the same magnitude for both foils.

Therefore a calculation of the forced vertical motions of the hydrofoils by means of the linear differential equation taking into account only the first harmonic excitation as done in the present report yields no satisfactory results. Further investigations specially with respect to nonlinearities and additional effects seem to be of great importance.

6. Nomenclature

c	chord length	
b	wetted semi-span of the hydrofoil	for the dihedral foil with respect to the undisturbed water surface
$A = \frac{2b}{c}$	wetted aspect ratio	
$\bar{h} = \frac{h}{c}$	nondimensional depth of the foil, defined as the distance between the undisturbed water surface and the centre of the meanline	
$\bar{h}_2 = \frac{\bar{h}_2}{c}$	likewise for the dihedral foil, defined in the plane of symmetry	
$m = \frac{f}{c}$	camber	
u_o	running speed	
u_W	speed of wave propagation	
$\lambda = \frac{2\pi u_W^2}{g}$	wave length for infinite depths	
a	wave amplitude	
γ	dihedral angle	
$\alpha_{geom.}$, α_g	geometrical angle of incidence	
ϱ	density of fluid	
P	weight of hydrofoil model including fixed part of measuring system (heave measurements)	
$\lvert z_F \rvert$	amplitude of heave of the hydrofoil	
$\lvert z_W \rvert$	amplitude of orbital motion	
K_A	aspect ratio-factor, steady state	see Part I
$K_{\bar{h}}$, $K_{\bar{h}_m}$	surface influence - factor	see Part I
K_α	angle of incidence-factor	see Part I
$\nu = \frac{g}{u_W 2}\ (u_o + u_W)$	frequency of encounter	
$\mu = \frac{\nu c}{2u_o}$	reduced frequency	
t	time	

7. References

[1] : : [5] see Part I

[6] Schwanecke, H. Über Messungen an periodisch instationär angeströmten Trag-Flügeln. Ingenieur-Archiv, Vol.30(1961), p. 350

[7] v.Kármán, Th./Sears, W.R. Airfoil theory for non-uniform motion. J.aeron.sc., Vol.5 (1938), p.379

Table 1

$\bar{h}$ = 1.20

μ [-]	u_o [m/s]	λ [m]	a [m]	ν [s^{-1}]	u_w (calc.) [m/s]	α_{geom} [deg]
0.081	6.04	5.85	0.0405	9.78	3.02	1.8
0.084	6.01	5.58	0.047	10.12	2.95	
0.092	6.04	4.98	0.056	11.10	2.79	
0.105	6.04	4.28	0.059	12.65	2.58	
0.112	6.00	3.94	0.0545	13.46	2.48	
0.126	6.02	3.57	0.0645	15.20	2.33	
0.142	6.08	2.99	0.062	17.25	2.16	
0.168	6.03	2.49	0.052	20.20	1.97	
0.208	6.02	1.96	0.040	25.05	1.75	
0.268	5.97	1.46	0.0255	32.05	1.51	1.8
0.080	6.02	5.92	0.041	9.62	3.04	1.6
0.272	5.99	1.66	0.0227	32.49	1.61	1.6

Table 2

$\bar{h}$ = 1.69

μ [-]	u_o [m/s]	λ [m]	a [m]	ν [s^{-1}]	u_w (calc.) [m/s]	α_{geom} [deg]
0.078	6.04	6.10	0.041	9.41	3.09	1.8
0.087	6.03	5.35	0.0515	10.56	2.89	
0.093	6.02	4.92	0.055	11.21	2.77	
0.102	6.03	4.43	0.0575	12.28	2.63	
0.117	6.06	4.00	0.0545	13.42	2.50	
0.127	6.02	3.42	0.0630	15.30	2.31	
0.144	6.01	2.96	0.0625	17.25	2.15	
0.168	5.93	2.49	0.0535	19.92	1.97	
0.194	6.03	2.10	0.0495	23.40	1.81	
0.252	6.05	1.56	0.0295	30.61	1.56	

Table 3

$\bar{h}$ = 2.19

μ [··]	u_o [m/s]	λ [m]	a [m]	ν [s^{-1}]	u_w (calc.) [m/s]	α_{geom} [deg]
0.079	6.03	5.97	0.0395	9.56	3.05	1.8
0.085	6.00	5.50	0.0495	10.20	2.93	
0.095	6.00	4.84	0.0575	11.30	2.75	
0.102	6.01	4.40	0.061	12.31	2.62	
0.102	5.99	4.40	0.059	12.25	2.62	
0.113	5.98	3.91	0.054	13.54	2.47	
0.127	6.02	3.42	0.062	15.22	2.31	
0.140	6.01	2.85	0.068	16.83	2.11	
0.158	6.01	2.66	0.0565	19.04	2.04	1.8
0.172	6.01	2.41	0.0545	20.62	1.94	2.3
0.195	6.04	2.10	0.0410	23.50	1.81	2.3
0.270	6.02	1.46	0.030	32.46	1.51	2.3

Table 4

$\bar{h}$ = 2.68

μ [··]	u_o [m/s]	λ [m]	a [m]	ν [s^{-1}]	u_w (calc.) [m/s]	α_{geom} [deg]
0.082	6.02	5.73	0.043	9.85	2.99	1.8
0.087	6.03	5.34	0.050	10.45	2.89	
0.093	6.02	4.94	0.0555	11.19	2.78	
0.100	6.02	4.66	0.061	12.00	2.70	
0.112	6.03	3.97	0.0585	13.46	2.49	
0.125	6.03	3.47	0.0650	15.09	2.33	
0.148	5.98	2.88	0.0555	17.73	2.12	
0.170	5.98	2.43	0.0485	20.40	1.95	
0.196	6.01	2.07	0.0485	23.65	1.80	
0.264	5.99	1.50	0.0295	31.61	1.53	

Table 5

$\bar{h}_2$ = 1.24

μ [--]	u_o [m/s]	λ [m]	a [m]	ν [s^{-1}]	u_w(calc.) [m/s]	α_{geom} [deg]
0.076	6.03	6.12	0.051	9.12	3.09	1.9
0.079	5.98	5.97	0.0405	9.50	3.05	
0.082	5.99	5.70	0.0425	9.85	2.98	
0.083	6.03	5.73	0.0620	9.98	2.99	
0.104	6.00	4.40	0.0645	12.44	2.62	
0.108	6.04	4.10	0.0590	13.20	2.53	
0.127	6.02	3.51	0.040	15.30	2.34	
0.149	5.99	2.91	0.0545	17.80	2.13	
0.167	6.02	2.52	0.0505	20.10	1.98	
0.207	6.02	1.96	0.0465	24.96	1.75	
0.246	6.06	1.62	0.0275	29.80	1.59	

Table 6

$\bar{h}_2$ = 1.74

μ [--]	u_o [m/s]	λ [m]	a [m]	ν [s^{-1}]	u_w(calc.) [m/s]	α_{geom} [deg]
0.078	6.03	6.08	0.0435	9.42	3.08	1.9
0.087	6.05	5.29	0.0575	10.50	2.87	
0.092	6.01	5.03	0.0590	11.00	2.80	
0.102	5.97	4.44	0.058	12.20	2.63	
0.111	6.00	4.02	0.059	13.40	2.50	
0.127	6.05	3.42	0.0655	15.30	2.31	
0.146	6.01	2.83	0.0625	17.60	2.10	
0.167	6.01	2.62	0.0525	20.10	2.02	
0.193	6.03	2.12	0.045	23.30	1.82	
0.259	6.04	1.52	0.0295	31.20	1.54	

Table 7

$\bar{h}_2 = 2.24$

μ [-]	u_o [m/s]	λ [m]	a [m]	ν [s^{-1}]	u_T (calc.) [m/s]	α_{geom} [deg]
0.081	6.03	5.77	0.0425	9.82	3.00	1°.9
0.085	6.01	5.50	0.0495	10.20	2.93	
0.093	6.02	5.10	0.056	11.20	2.82	
0.102	6.07	4.50	0.058	12.40	2.65	
0.112	6.05	3.98	0.055	13.50	2.49	
0.112	6.04	3.96	0.061	13.50	2.49	
0.125	6.04	3.48	0.067	15.10	2.33	
0.126	6.03	3.51	0.0655	15.20	2.34	
0.147	6.00	2.88	0.0655	17.70	2.12	
0.169	6.01	2.43	0.0535	20.40	1.95	
0.202	6.01	2.01	0.050	24.40	1.77	
0.263	5.99	1.50	0.0245	31.50	1.53	

Table 8

$\bar{h}$ = 0.50

μ [-]	u_0 [m/s]	z_0 [m]	ν [s^{-1}]
0.078	4.99	0.0105	7.78
0.110	4.97	0.0105	10.95
0.120	4.99	0.0105	11.99
0.147	4.99	0.0105	14.72
0.174	4.99	0.0105	17.43
0.196	4.99	0.0105	19.59
0.220	4.99	0.0105	21.96
0.241	4.99	0.0105	24.13
0.280	4.99	0.0105	28.00

Table 9

$\bar{h}$ = 0.98

μ [-]	u_0 [m/s]	z_0 [m]	ν [s^{-1}]
0.084	4.99	0.010	8.36
0.106	5.01	0.010	10.60
0.122	4.99	0.010	12.17
0.143	4.99	0.010	14.32
0.158	4.99	0.010	15.80
0.171	4.99	0.010	17.14
0.189	4.99	0.010	18.92
0.219	4.99	0.010	21.93
0.224	4.99	0.010	22.42
0.232	4.99	0.010	23.18
0.302	4.99	0.00525	30.24

Table 10

$\bar{h}$ = 1.48

μ [-]	u_0 [m/s]	z_0 [m]	ν [s^{-1}]
0.076	4.97	0.0100	7.60
0.094	4.97	0.0100	9.34
0.105	4.99	0.0100	10.51
0.116	4.99	0.00650	11.60
0.143	4.99	0.00650	14.28
0.161	4.99	0.00650	16.09
0.184	4.97	0.00650	18.33
0.198	4.97	0.00375	19.70
0.177	4.97	0.00375	17.54
0.239	4.97	0.00375	23.75
0.306	4.97	0.00375	30.39

Table 11

$\bar{h}$ = 1.85

μ [-]	u_0 [m/s]	z_0 [m]	ν [s^{-1}]
0.070	4.97	0.0200	7.00
0.102	4.99	0.01575	10.14
0.127	4.97	0.0090	12.56
0.142	4.97	0.0055	14.15
0.166	4.99	0.0055	16.57
0.190	4.99	0.00375	18.93
0.260	4.97	0.00375	25.88
0.214	4.97	0.00375	21.21
0.267	4.97	0.00375	26.53

Table 12

$\bar{h}_2$= 0.50

μ [-]	u_0 [m/s]	z_0 [m]	ν [s^{-1}]
0.069	4.99	0.0085	6.83
0.105	4.99	0.0085	10.47
0.134	5.01	0.0085	13.47
0.146	5.02	0.0085	14.74
0.163	4.99	0.0085	16.27
0.176	4.98	0.0085	17.56
0.192	4.99	0.0085	19.24
0.228	4.98	0.0085	22.76
0.256	4.99	0.0085	25.56
0.275	4.98	0.0085	27.48
0.296	5.01	0.0085	29.60
0.302	4.98	0.0085	30.24

Table 13

$\bar{h}_2$= 1.00

μ [-]	u_0 [m/s]	z_0 [m]	ν [s^{-1}]
0.075	4.99	0.0085	7.54
0.105	4.97	0.0085	10.47
0.123	4.98	0.0085	12.28
0.153	4.98	0.0085	15.25
0.168	4.98	0.0085	16.82
0.177	4.97	0.0085	17.64
0.200	5.02	0.0085	20.13
0.228	5.02	0.0085	22.95
0.258	5.02	0.0085	25.95
0.300	4.97	0.0085	29.80

Table 14

$\bar{h}_2$= 1.45

μ [-]	u_0 [m/s]	z_0 [m]	ν [s^{-1}]
0.069	4.99	0.0085	6.90
0.088	4.98	0.0085	8.75
0.108	4.97	0.0085	10.80
0.129	4.98	0.0085	12.90
0.159	4.98	0.0085	15.94
0.160	4.99	0.0085	16.02
0.190	4.97	0.0085	18.98
0.227	4.98	0.0085	22.67
0.243	4.98	0.0085	24.34
0.242	4.98	0.0085	24.24

Table 15

$\bar{h}_2$= 2.00

μ [-]	u_0 [m/s]	z_0 [m]	ν [s^{-1}]
0.074	4.97	0.00475	7.39
0.097	4.97	0.00475	9.71
0.117	4.99	0.00475	11.70
0.135	4.97	0.00475	13.51
0.139	4.98	0.00475	13.89
0.176	4.98	0.00475	17.62
0.206	4.97	0.00475	20.59
0.233	4.97	0.00475	23.30

Table 16

Flat foil

μ [··]	u_o [m/s]	λ [m]	a [m]	ν [s^{-1}]	u_w (calc.) [m/s]
0.079	5.82	6.08	0.0655	9.21	3.08
0.096	5.82	4.80	0.0780	10.93	2.74
0.108	5.86	4.16	0.1075	12.75	2.55
0.113	5.86	3.96	0.0615	13.24	2.49
0.127	5.80	3.47	0.0915	14.70	2.33
0.144	5.80	2.95	0.0635	16.88	2.15
0.197	5.80	2.10	0.0535	22.94	1.81
0.253	5.80	1.56	0.0320	29.67	1.56
0.283	5.82	1.38	0.0228	32.94	1.47

Table 17

Dihedral foil

μ [··]	u_o [m/s]	λ [m]	a [m]	ν [s^{-1}]	u_w (calc.) [m/s]
0.078	6.05	6.02	0.0573	9.49	3.07
0.080	6.06	5.87	0.0543	9.72	3.03
0.098	5.99	4.76	0.0510	11.50	2.73
0.110	5.97	4.00	0.0548	13.21	2.50
0.113	5.97	3.96	0.0535	13.45	2.49
0.143	6.00	2.98	0.0603	17.16	2.16
0.169	6.01	2.44	0.0435	20.46	1.95
0.210	6.01	2.03	0.0403	25.12	1.78
0.247	5.99	1.60	0.0345	29.74	1.58
0.386	6.00	1.03	0.012	46.0	1.3

1. Two-component measuring device
2. Model (dihedral foil)
3. Wave recorder

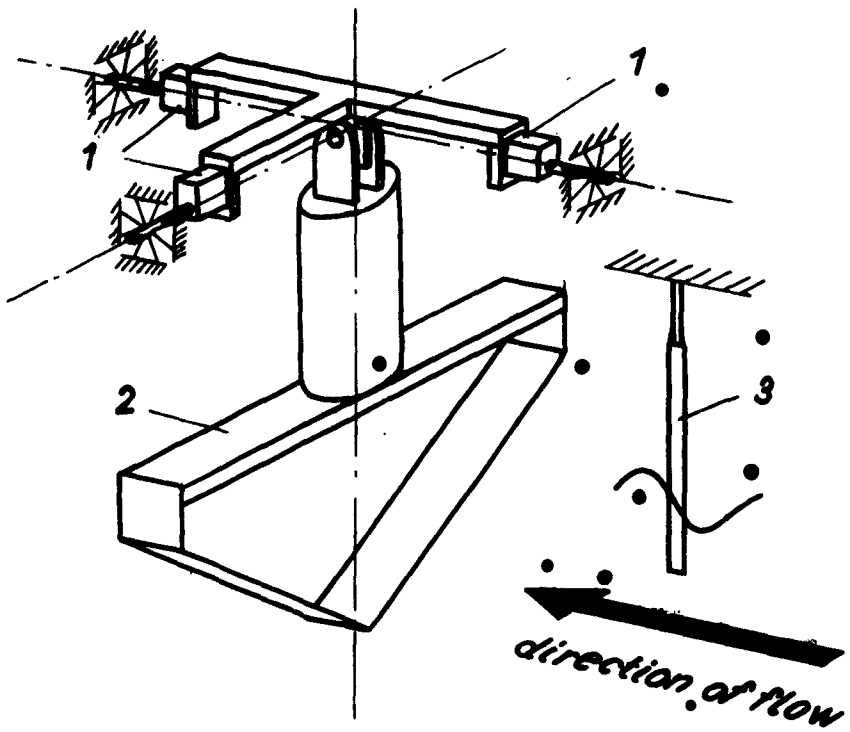

measuring apparatus for exciting forces (schematical)

fig. 1

1. Heave measuring device
2. Heave generator
3. Supporting tube
4. Lift measuring device
5. Model (dihedral foil)
6. vertical accelerometer

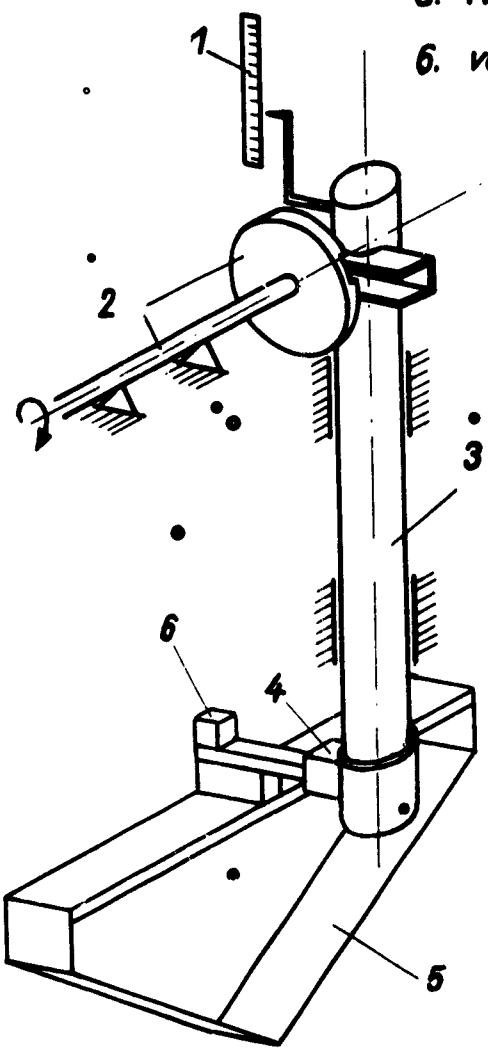

direction of flow

measuring apparatus for added masses and damping forces (schematical)

fig. 2

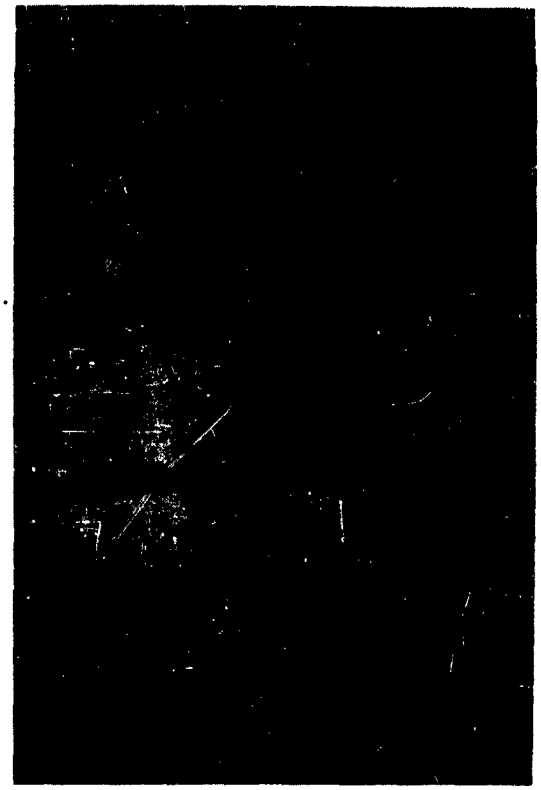

3

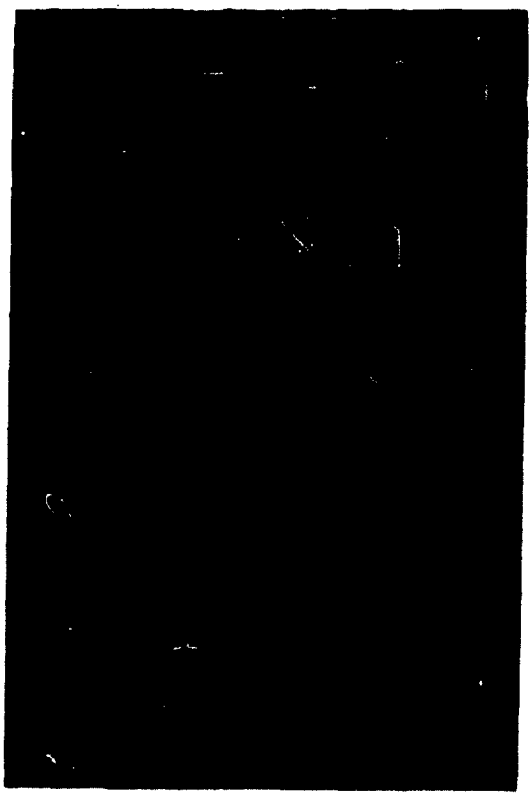

4

measuring arrangements for exciting forces and for added masses and damping forces

fig.3,4

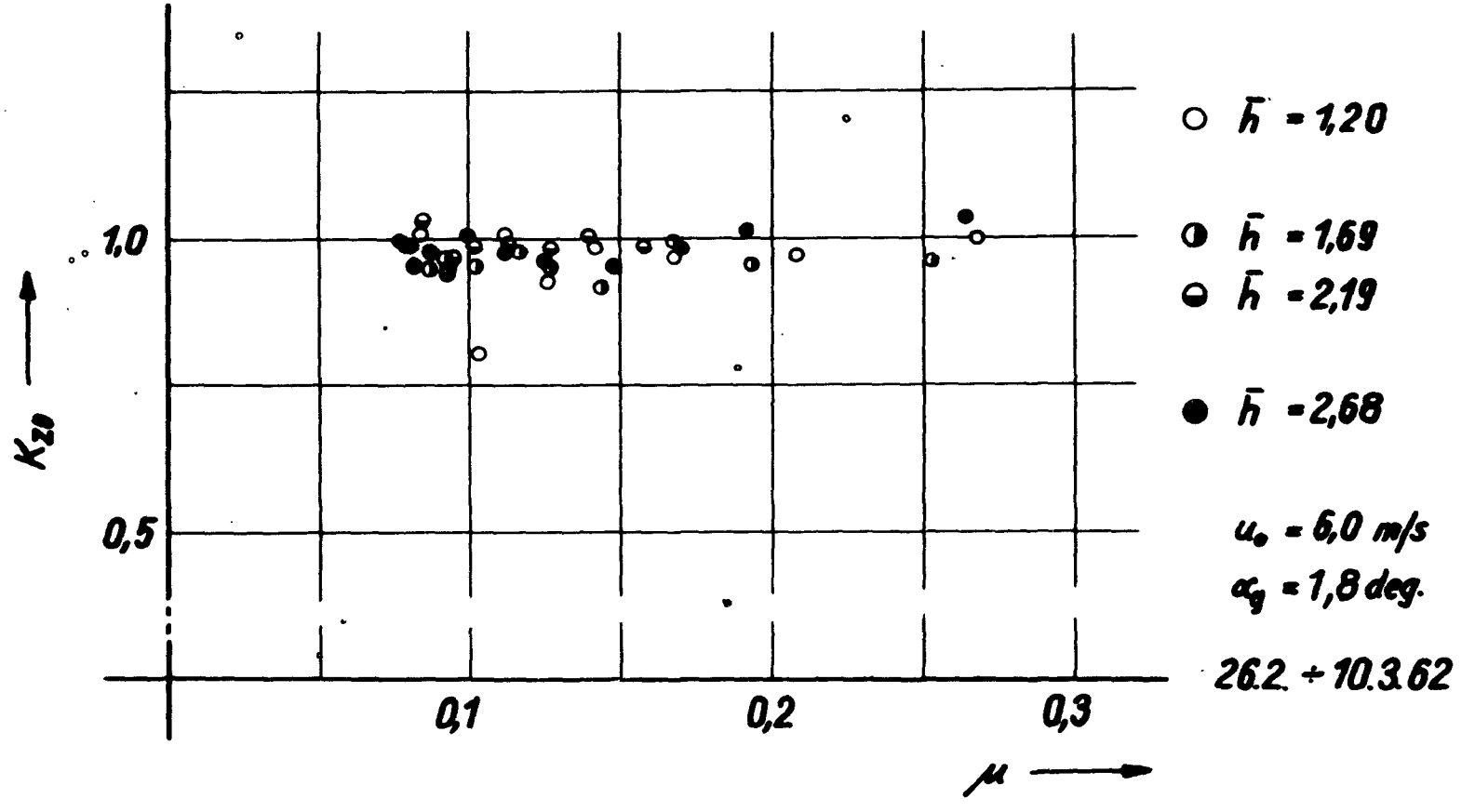

flat foil	coefficient of steady-state lift	fig.5

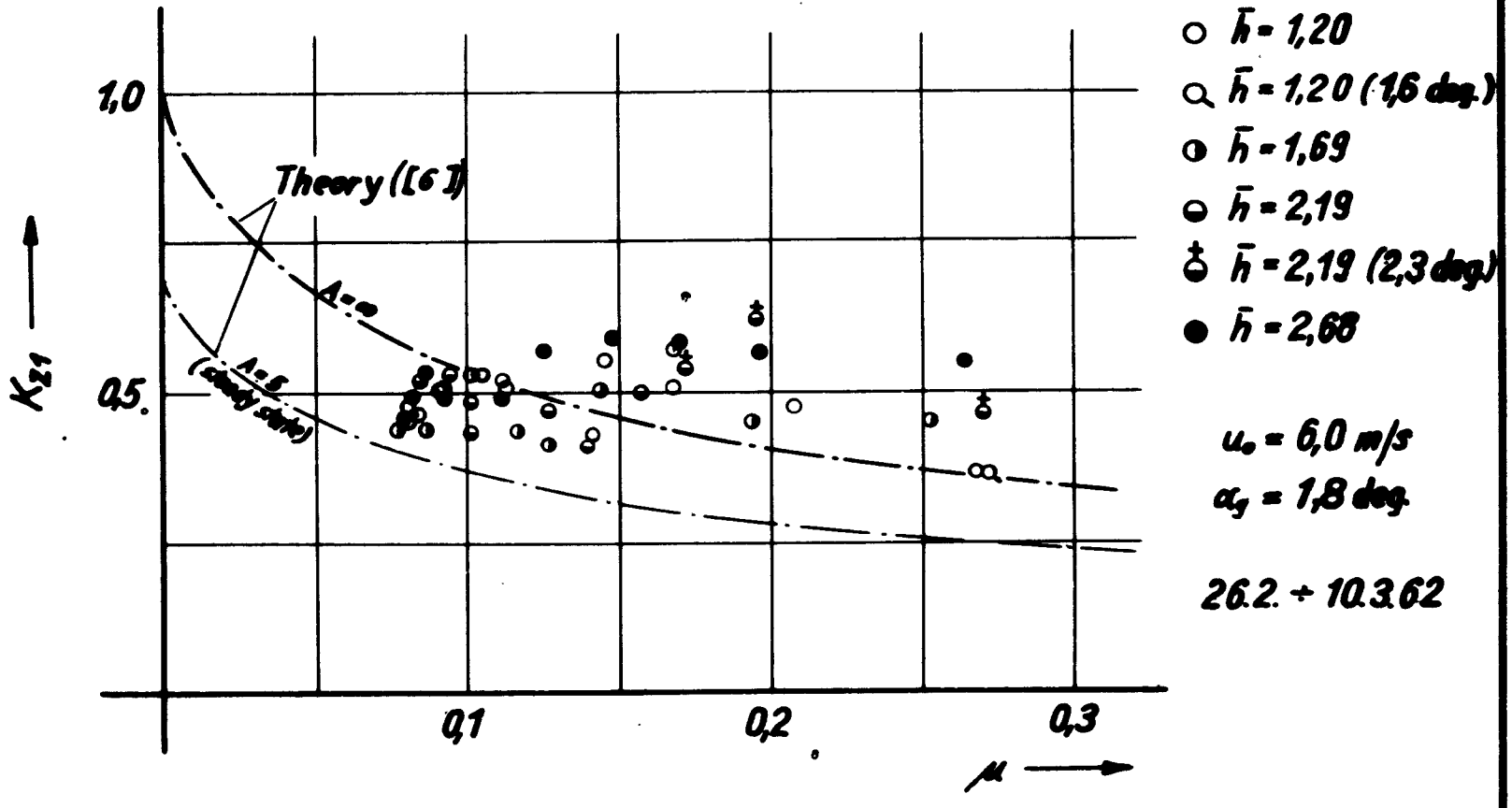

flat foil	coefficient of first order unsteady lift	fig. 6

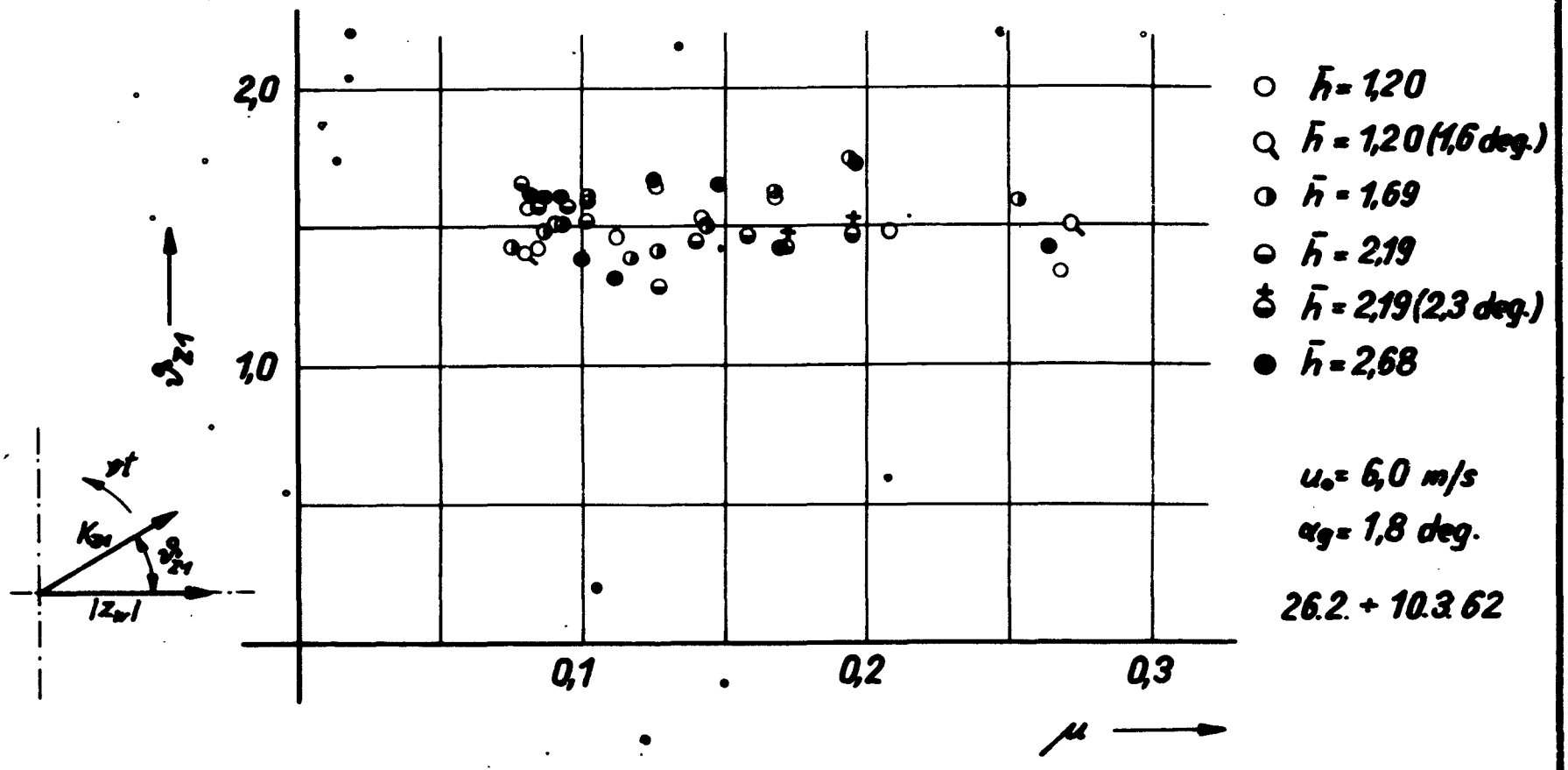

flat foil	phase angle between wave peak and maximum of first order unsteady lift	fig. 7

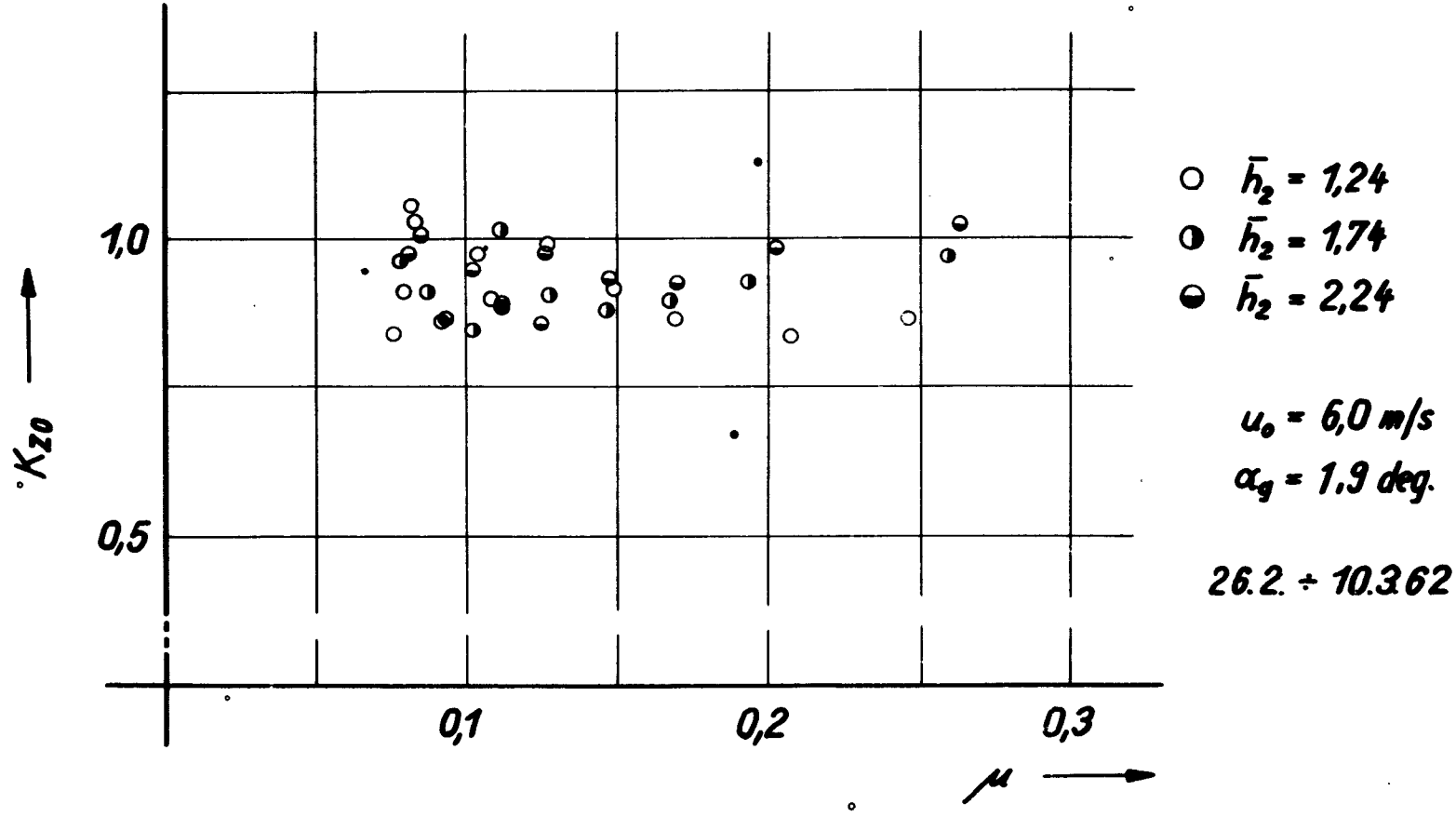

dihedral foil	coefficient of steady-state lift	fig. 8

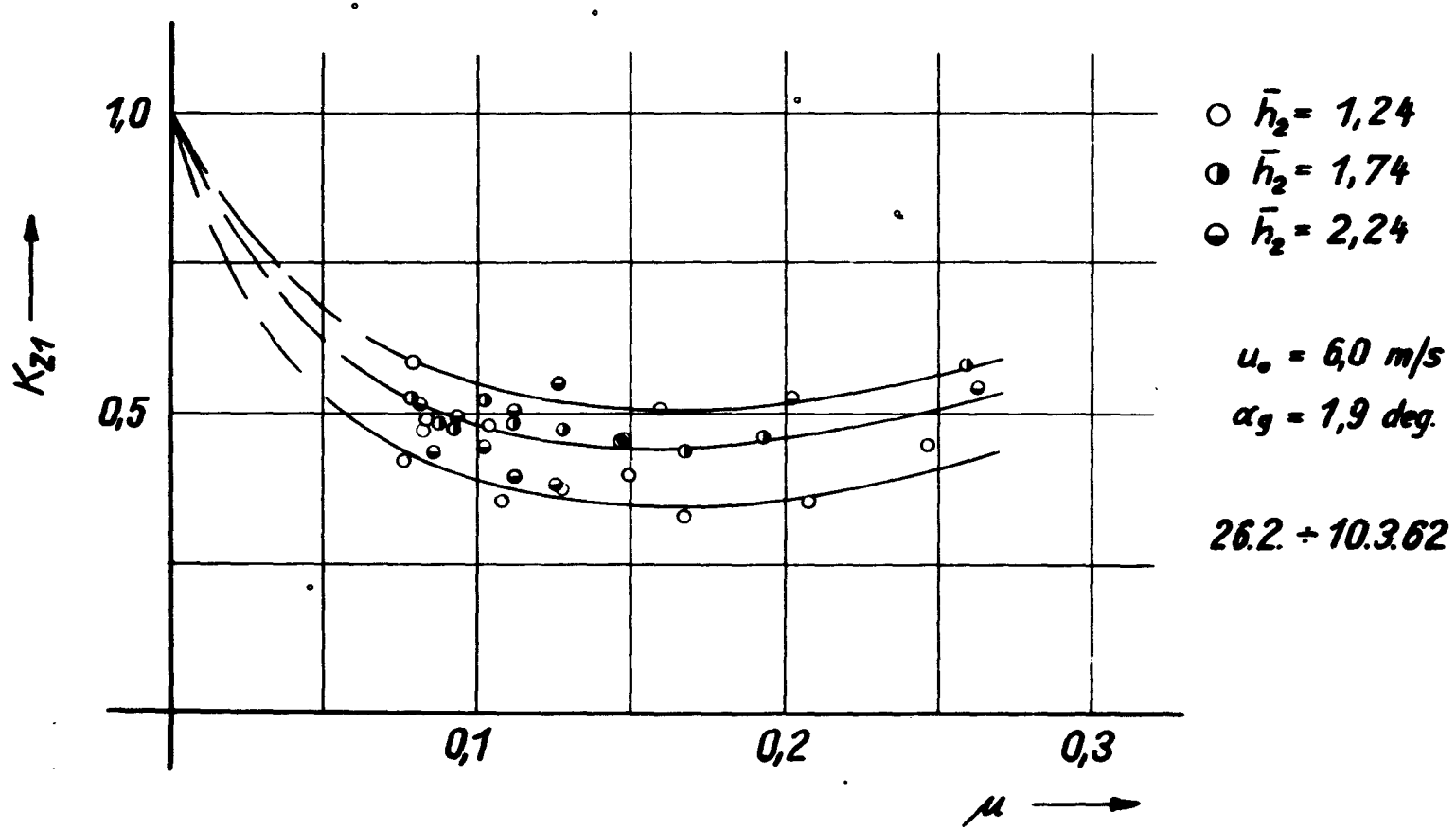

dihedral foil	coefficient of first order unsteady lift	fig. 9

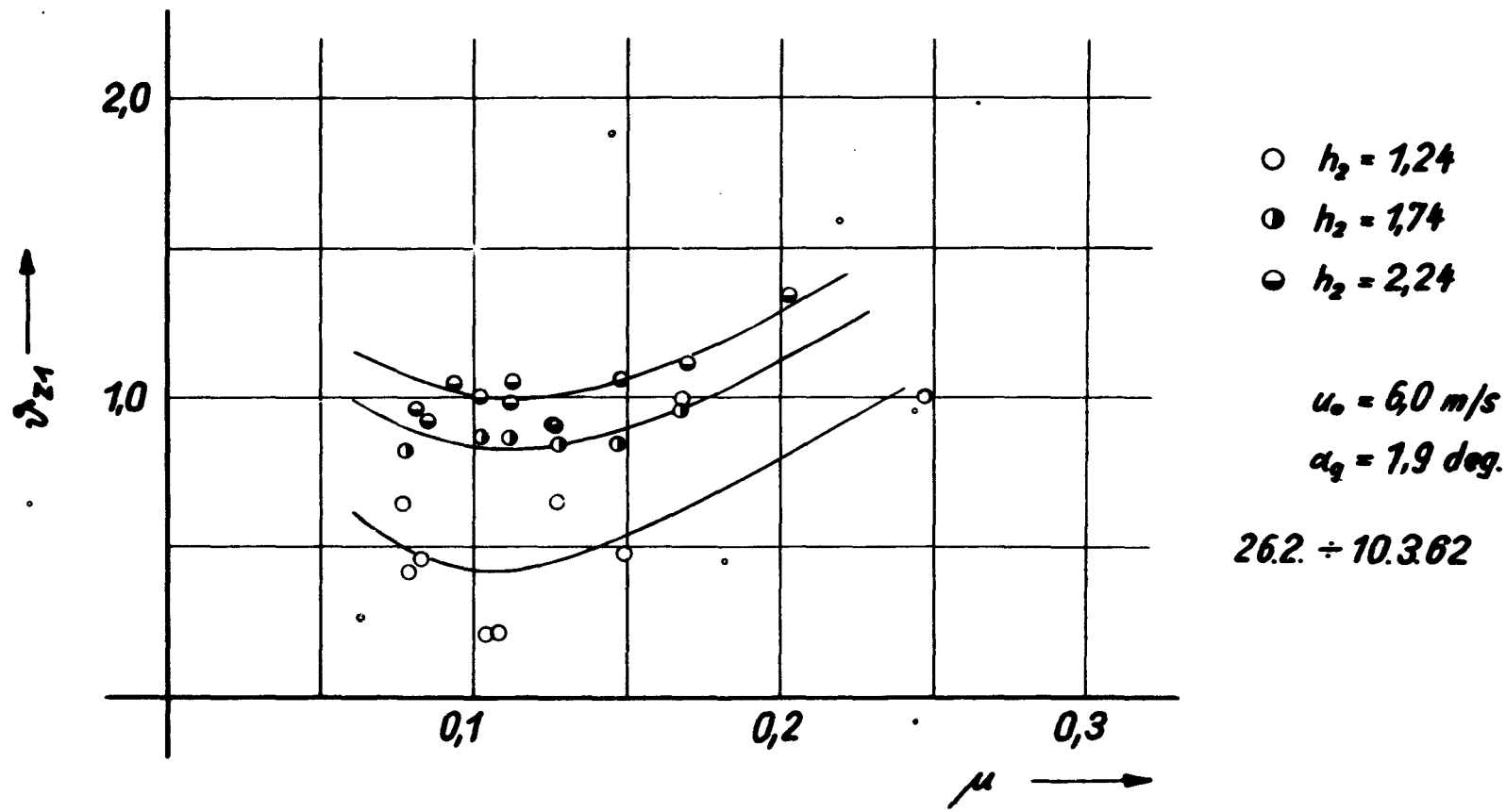

dihedral foil	phase angle between wave peak and maximum of first order unsteady lift	fig. 10

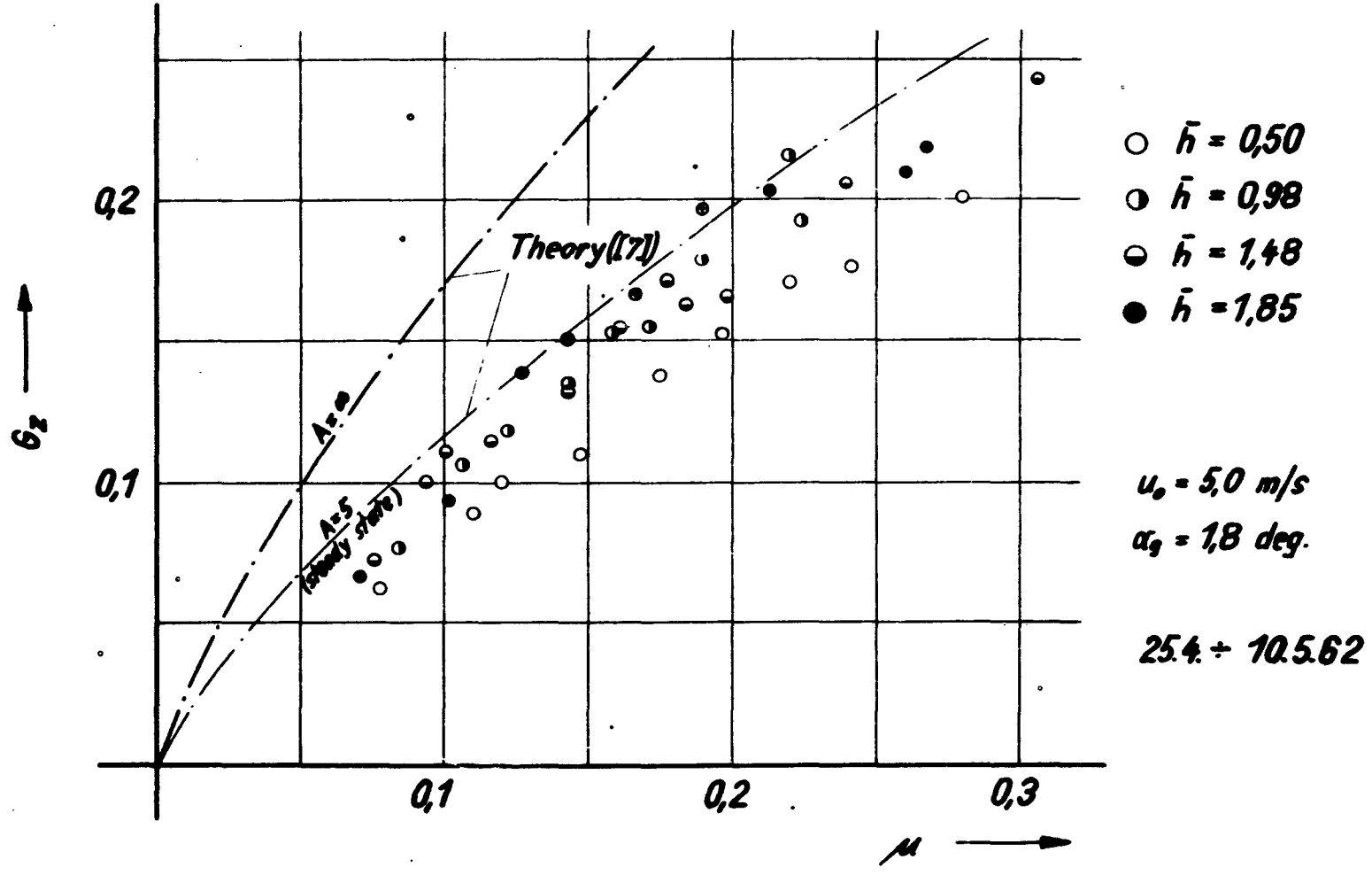

flat foil	amplitudes of unsteady lift due to vertical oscillation	fig. 11

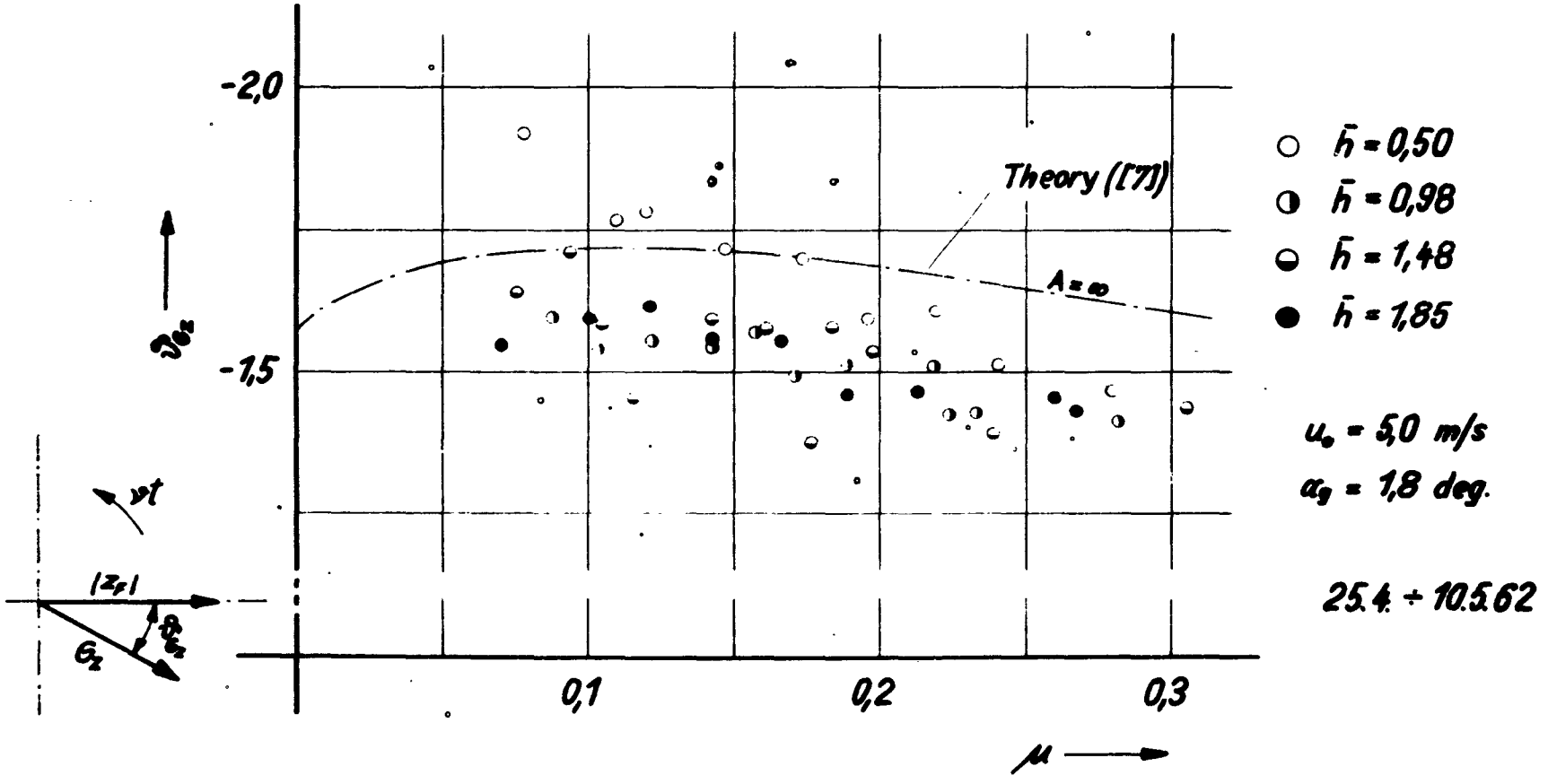

flat foil	phase angle between vertical oscillation and unsteady lift	fig 12

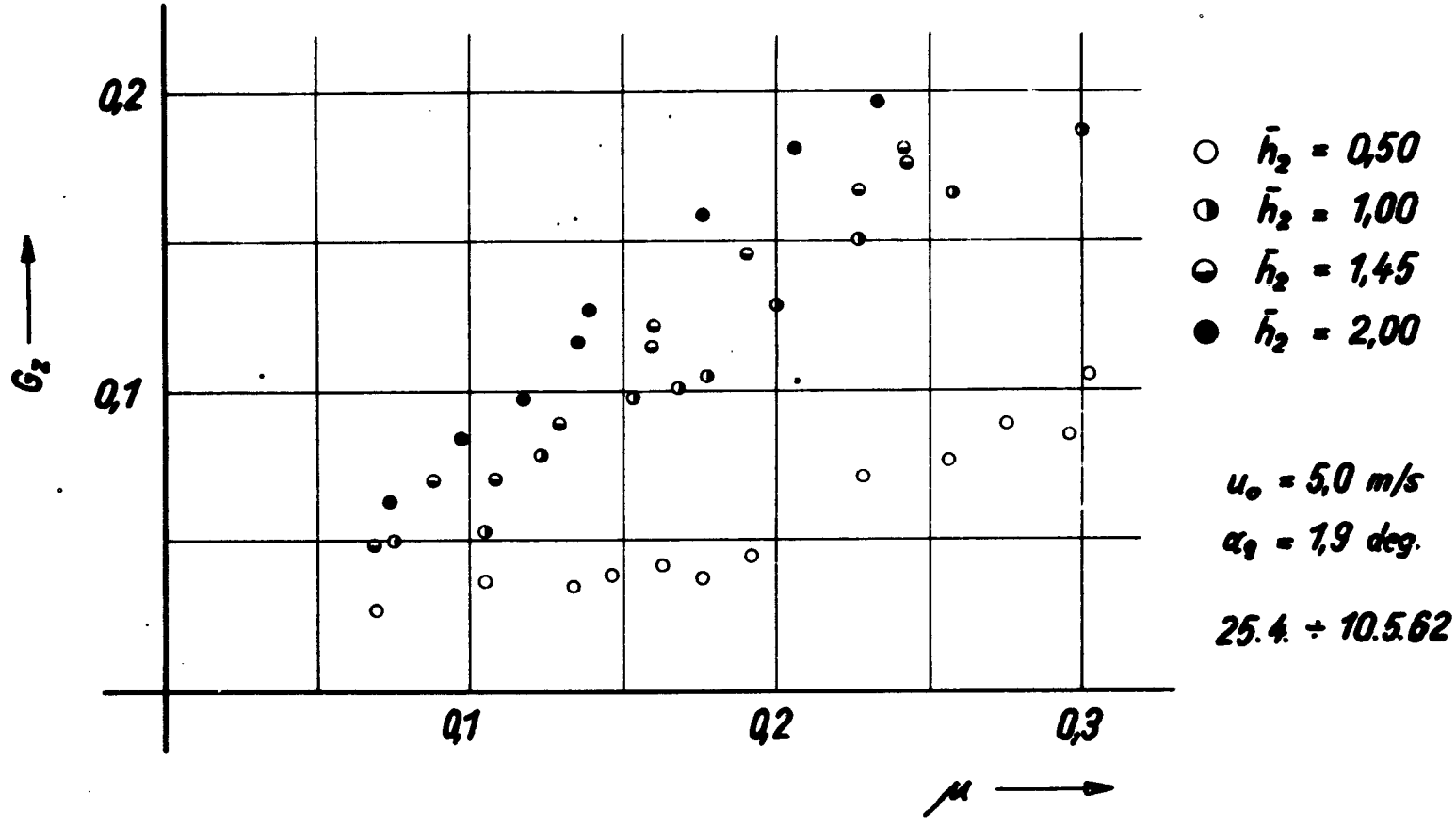

dihedral foil	amplitudes of unsteady lift due to vertical oscillation	fig 13

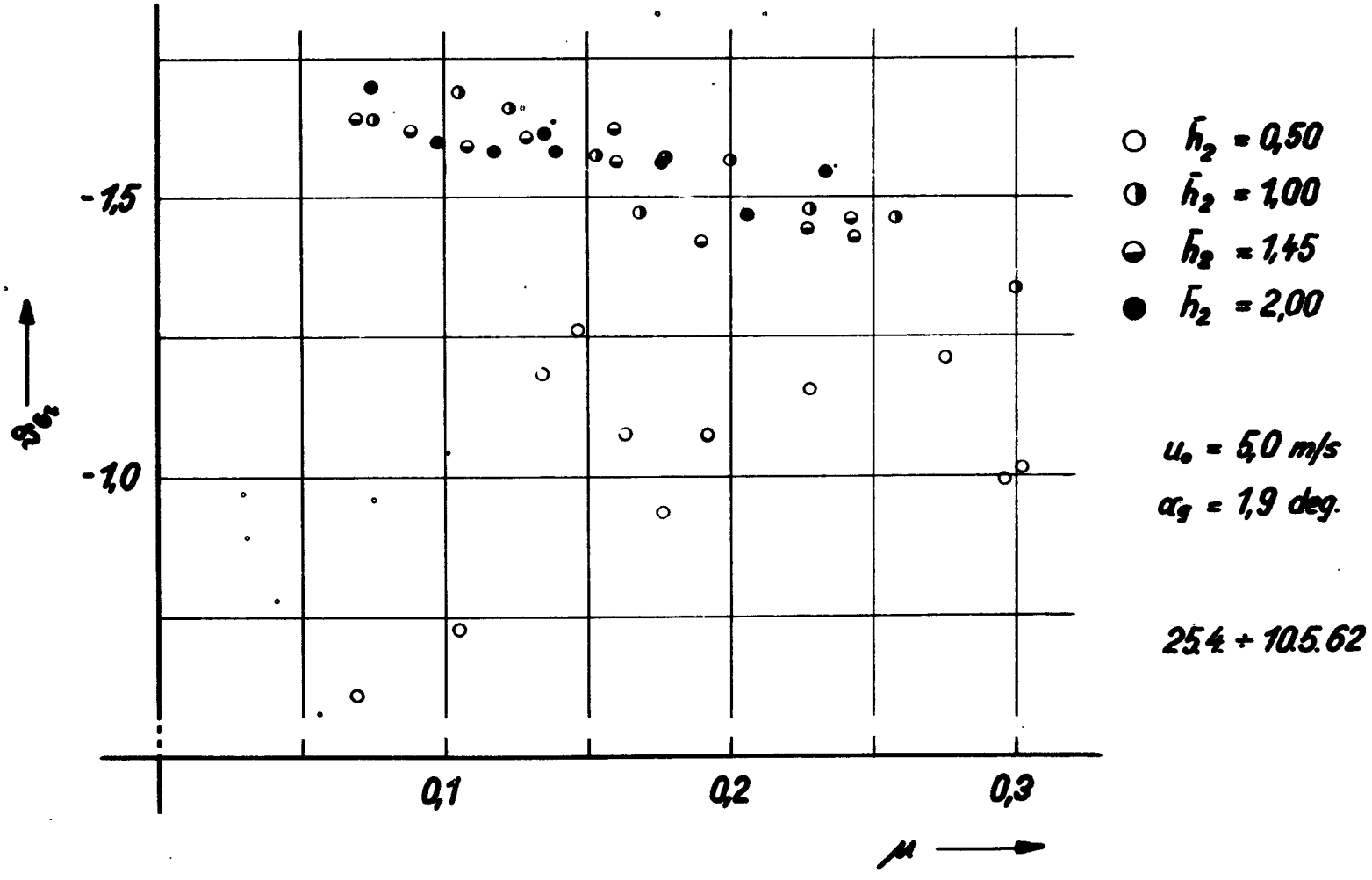

dihedral foil	phase angle between vertical oscillation and unsteady lift	fig. 14

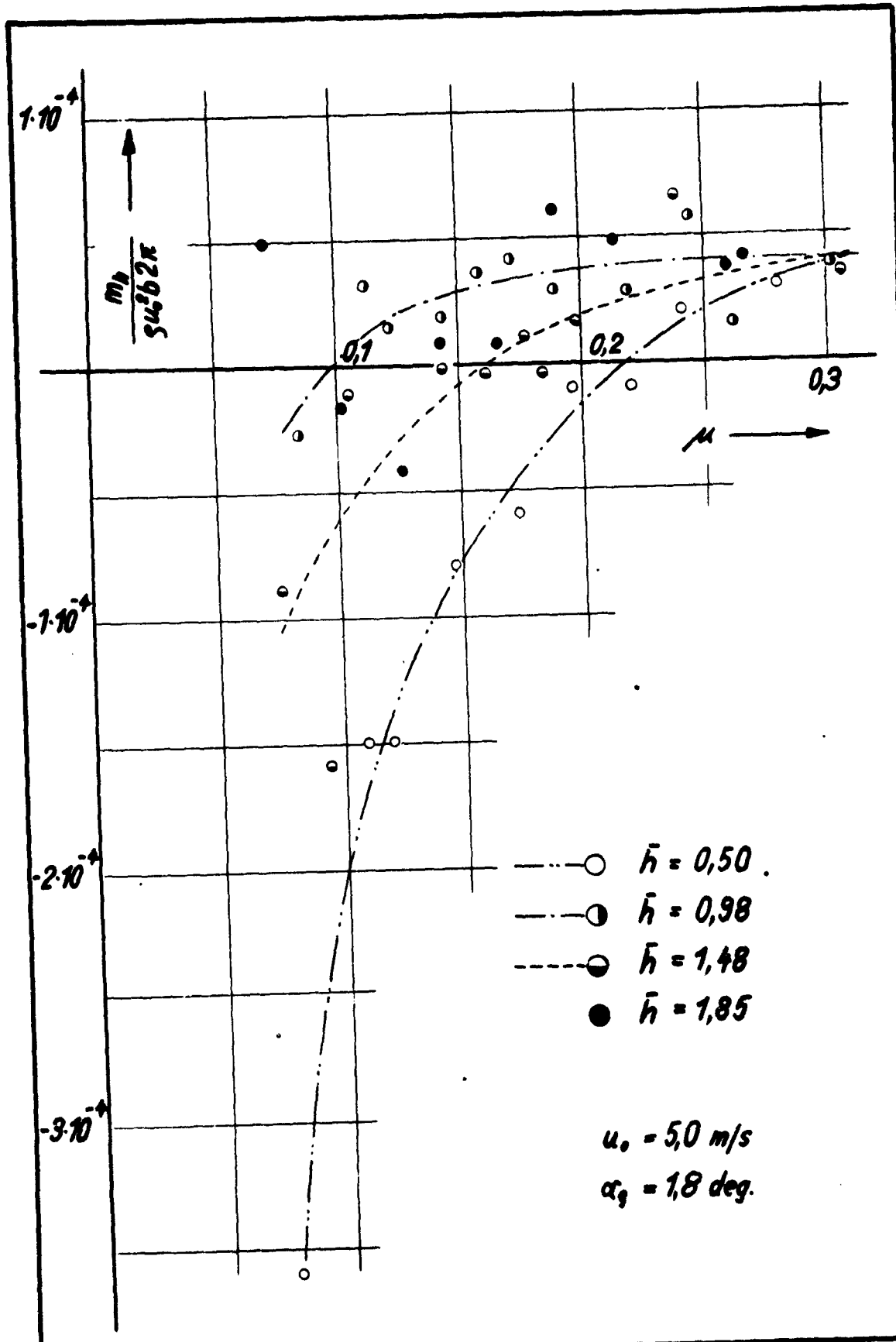

flat foil	hydrodynamic masses	fig. 15

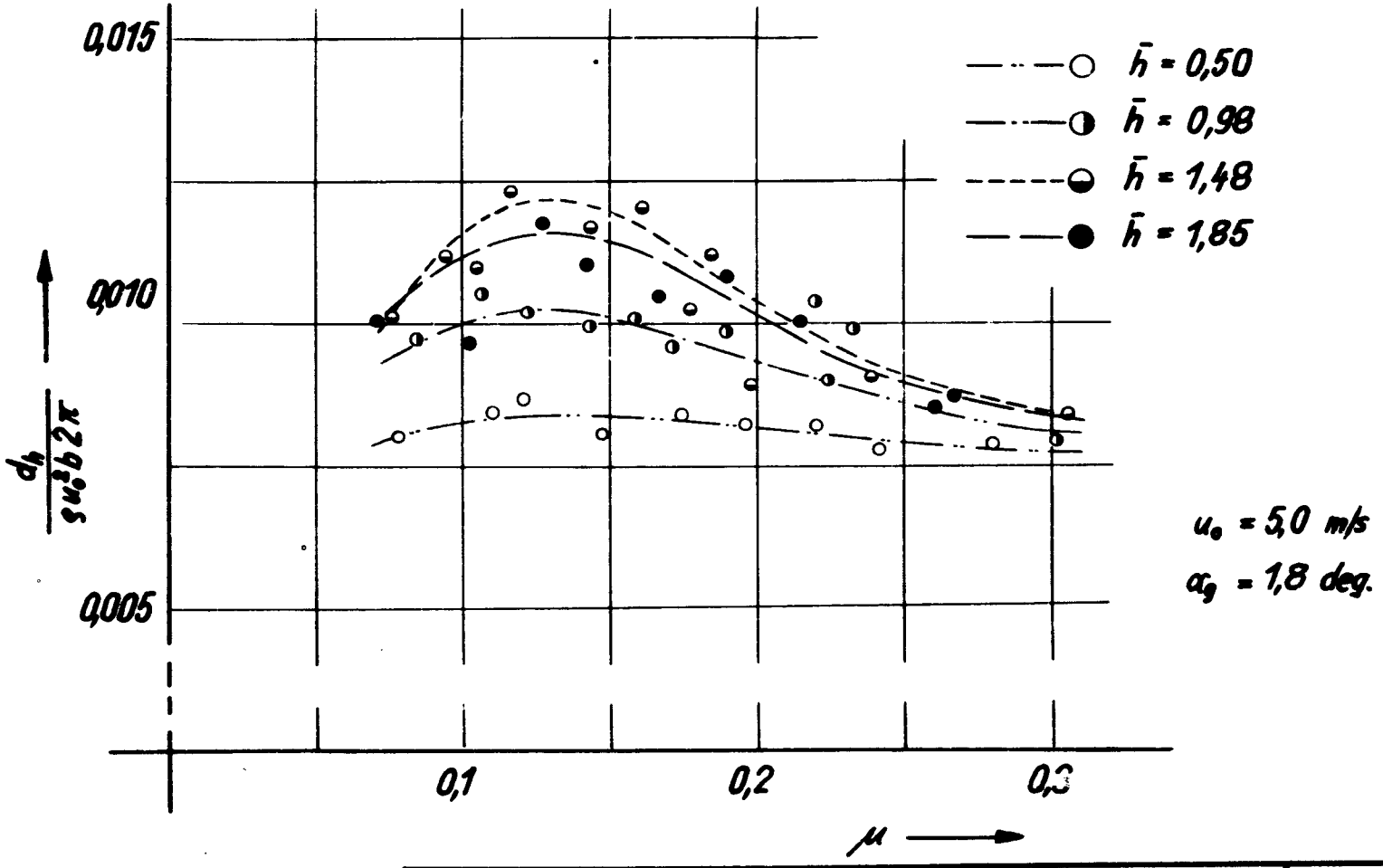

flat foil	hydrodynamic damping forces	fig. 16

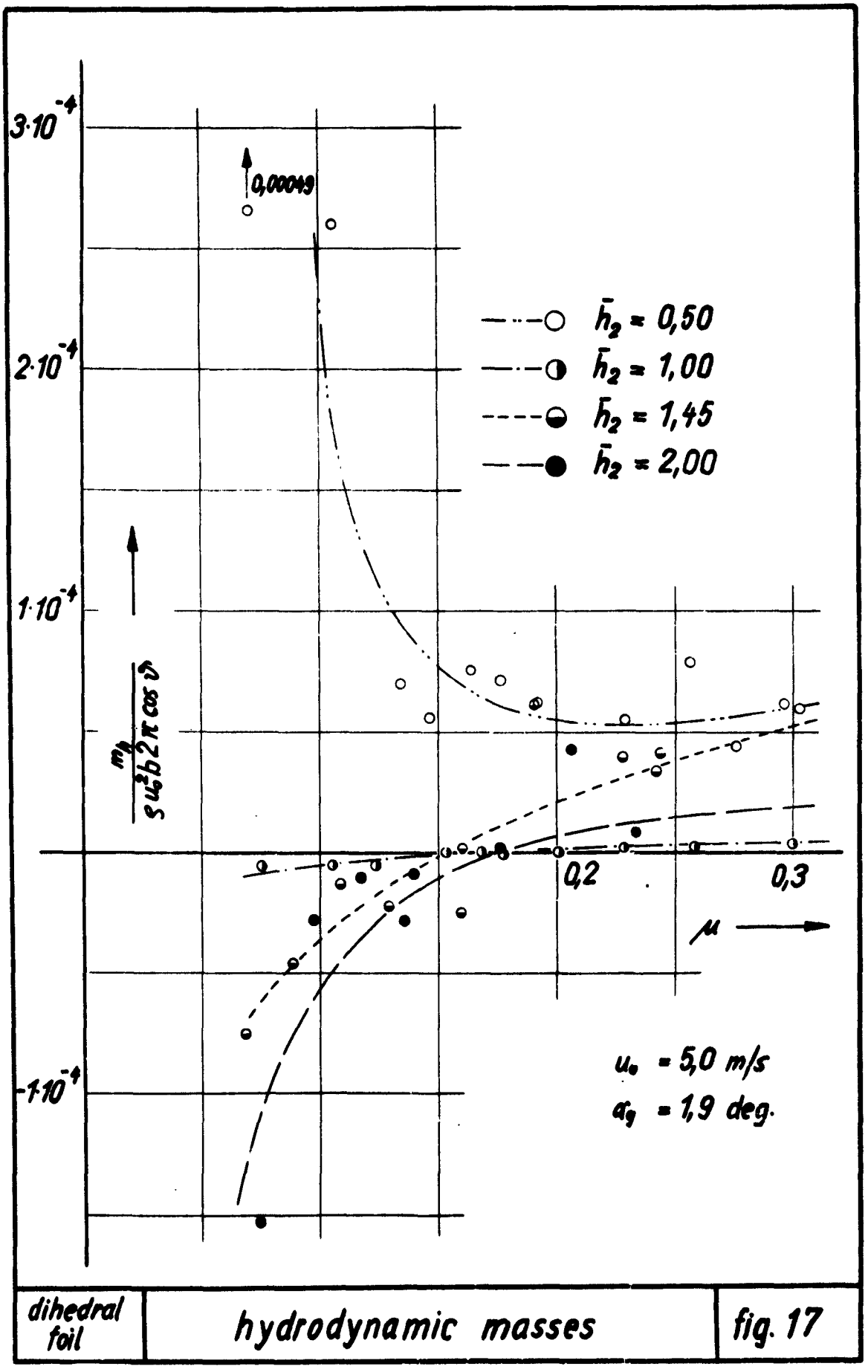

dihedral foil	hydrodynamic masses	fig. 17

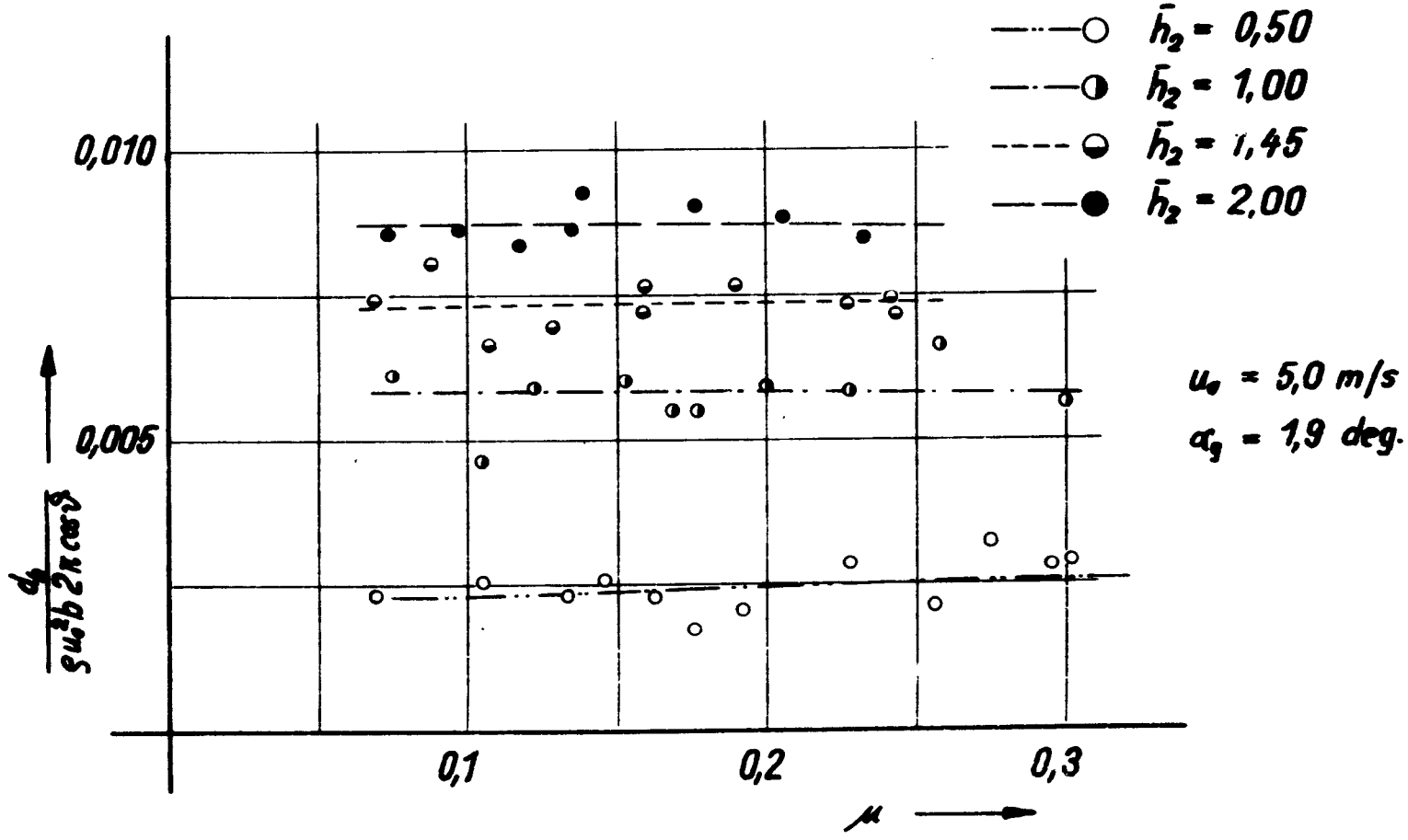

dihedral foil	hydrodynamic damping forces	fig. 18

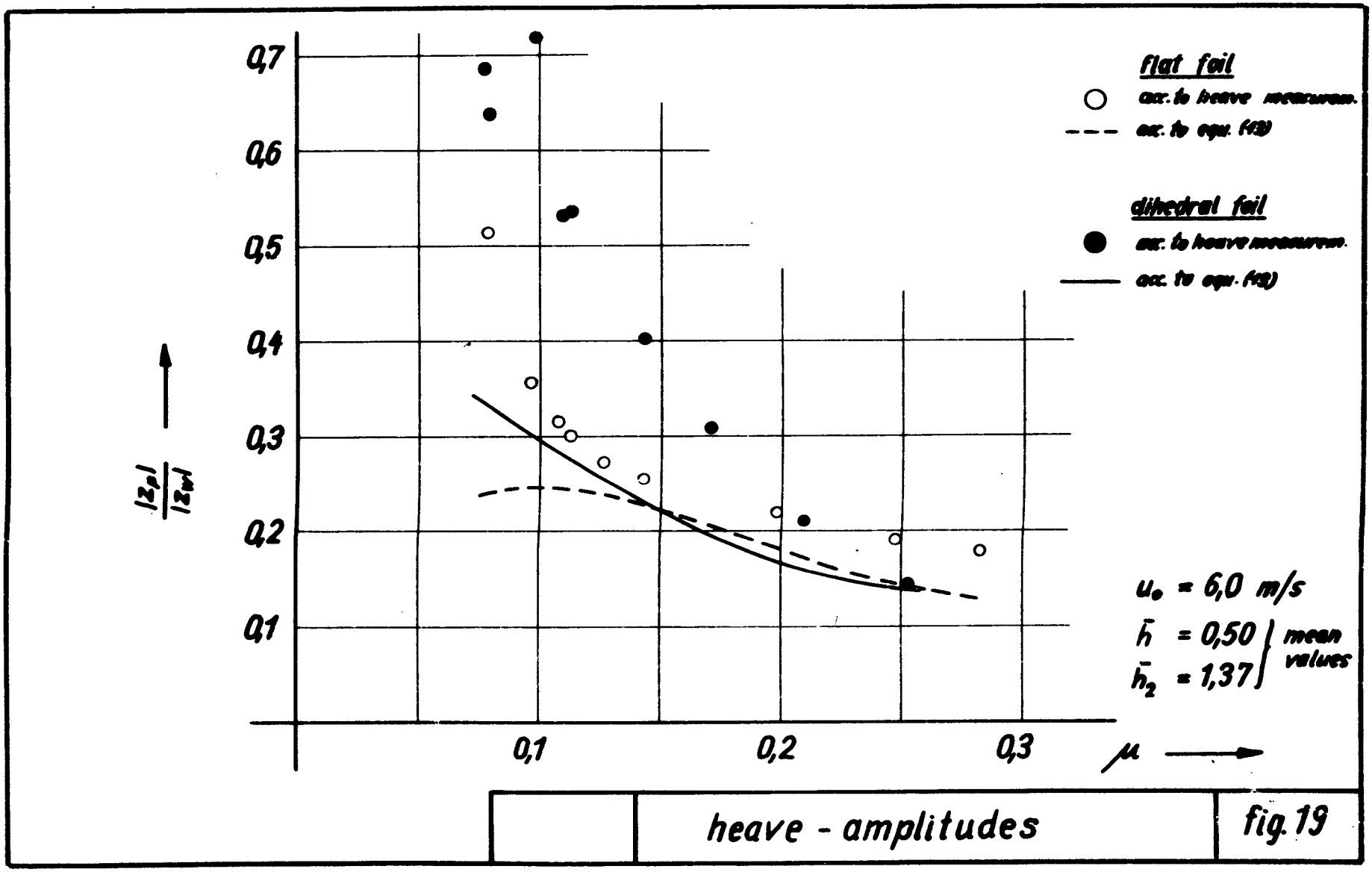

heave - amplitudes

fig. 19

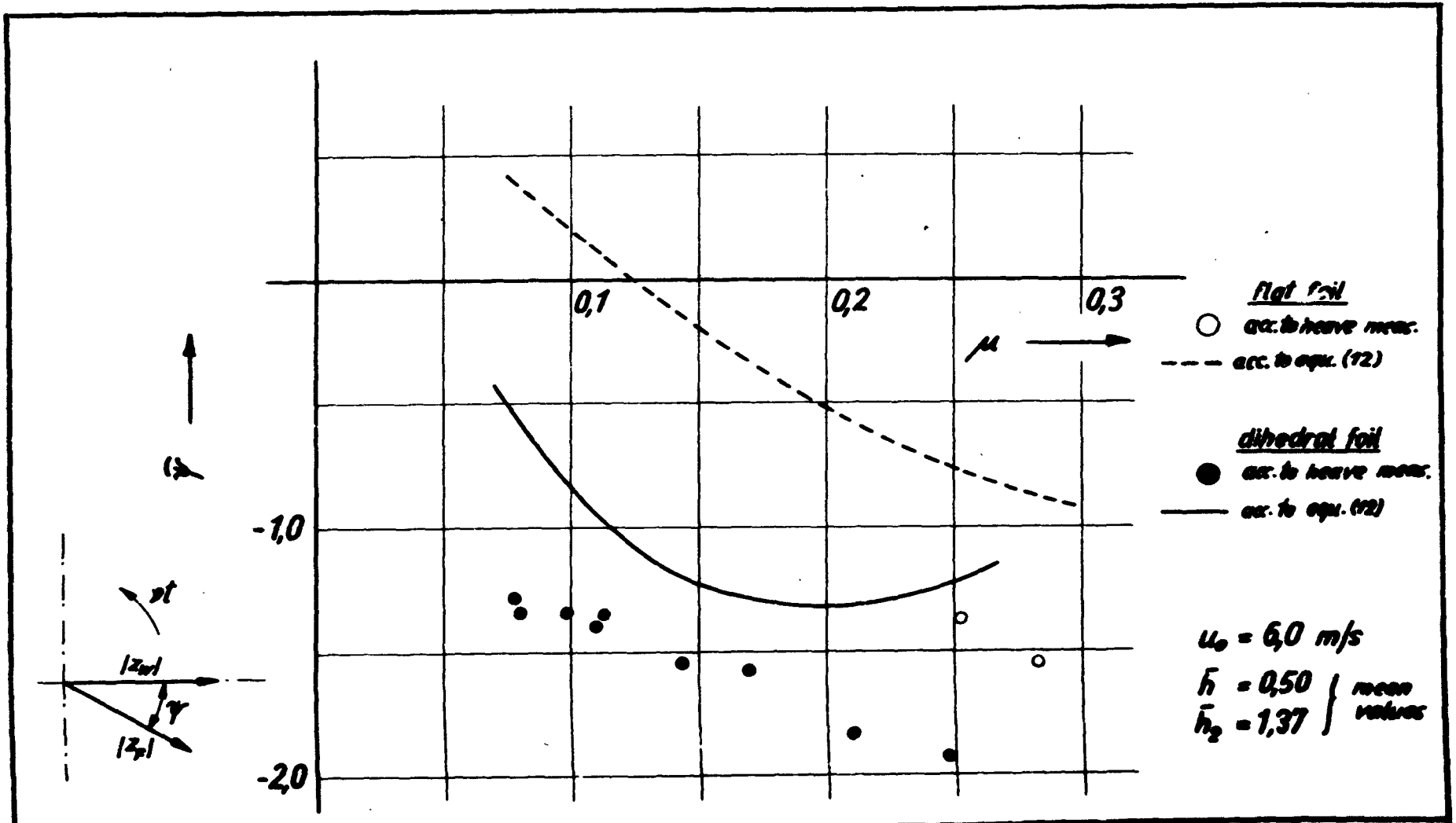

phase-angle of heaving

fig. 20